ELSEVIER

Materials Science and Engineering A260 (1999) 41–47

MATERIALS SCIENCE & ENGINEERING A

Interaction of local elastoplasticity with hydrogen: embrittlement effects

P. Sofronis *, J. Lufrano

Department of Theoretical and Applied Mechanics and Materials Research Laboratory, University of Illinois at Urbana-Champaign, Urbana, IL 61801, USA

Accepted 18 August 1998

Abstract

The finite element method was used to solve the coupled elastic–plastic boundary value problem and transient hydrogen diffusion initial boundary value problem. Solutions were obtained at room temperature and under plane strain deformation in the neighborhood of a blunting crack tip under small scale yielding conditions and in the neighborhood of a rounded notch in a 4-point bend specimen. A discussion of the finite element results in conjunction with different mechanisms of hydrogen embrittlement is presented. If a critical amount of hydrogen is required for hydrogen induced crack initiation, the present results predict locations of crack initiation sites at steel bend specimens which are in agreement with experimental observations on the occurrence of the first microcracking event.

Keywords: Transient hydrogen diffusion; Plane strain deformation; Blunting crack tip; Microcracking event

1. The hydrogen transport equation in an elastoplastically strained material

Following Sofronis and McMeeking [1], one can state the governing equation for transient hydrogen diffusion accounting for trapping and hydrostatic drift as [2]

$$\frac{D}{D_{\text{eff}}}\frac{\mathrm{d}C_{\text{L}}}{\mathrm{d}t}=DC_{\text{L},ii}-\left(\frac{DV_{\text{H}}C_{\text{L}}}{3RT}\sigma_{kk,i}\right)_{,i} \tag{1}$$

where C_{L} is the hydrogen concentration in normal interstitial lattice sites (NILS), D is the hydrogen diffusion constant through NILS, D_{eff} is an effective diffusion constant given by $D_{\text{eff}}=D/(1+\partial C_{\text{T}}/\partial C_{\text{L}})$, C_{T} is the hydrogen concentration in trapping sites, V_{H} is the partial molar volume of hydrogen in solid solution, σ_{ij} is the Cauchy stress, R is the gas constant equal to 8.31 J mol^{-1} K^{-1}, T is the absolute temperature, $(\ )_{,i}=\partial(\ )/\partial x_i$, $\mathrm{d}/\mathrm{d}t$ is the time derivative, and the standard summation convention over the range is implied for a repeated index. Concentrations C_{L} and C_{T} are measured in hydrogen atoms per unit volume.

The material is assumed to be linearly elastic and isotropic with moduli independent of the local hydrogen concentration. Under plastic straining, it hardens isotropically and flows according to von-Mises J_2 flow theory. The associated flow law is given by the classical Prandtl-Reuss equations [3]. The total deformation rate, $\mathrm{D}_{ij}=(v_{i,j}+v_{j,i})/2$, where v_i is the component of the velocity, is expressed as $D_{ij}=\mathrm{D}^{\text{e}}_{ij}+D^{\text{p}}_{ij}+D^{\text{t}}_{ij}$ where D^{e}_{ij} denotes the elastic part, D^{p}_{ij} is the plastic part, and D^{t}_{ij}, denotes the part due to lattice straining by the solute hydrogen. In the context of large strain formulation, the hydrogen induced deformation rate, which is purely dilatational [4], is phrased as

$$D^{\text{t}}_{ij}=\frac{\mathrm{d}}{\mathrm{d}t}\left[\ln\left(1+\frac{c\Delta v}{3\Omega}\right)\right]\delta_{ij'} \tag{2}$$

where c is total hydrogen concentration measured in hydrogen atoms per solvent atom, Δv is the volume change per atom of hydrogen introduced into solution that is directly related to the partial molar volume of hydrogen $V_{\text{H}}=\Delta v N_{\text{A}}$ in solution, and Ω is the mean atomic volume of the host metal atom.

The problem of calculating the strain field and the local distribution of hydrogen is coupled in a non-linear sense and the solution procedure involves iteration

* Corresponding author. Tel. +1-217-3332636; fax: +1-217-2445707; e-mail: sofronis@uiuc.edu.

0921-5093/99/$ - see front matter
PII: S0921-5093(98)00982-4

[1,5,6]. The finite element procedures for the solution of the coupled problems are outlined in the work by Sofronis and McMeeking [1] and Lufrano [7]. The formulation of Govindarajan and Aravas [8] for large strain plasticity was adopted to ensure zero lattice strain during large rigid body rotation.

2. Finite element calculation results of the transient hydrogen distribution

The transient hydrogen distribution as affected by initial concentration and levels of hydrostatic stress and plastic strain (through trapping) is monitored at the neighborhood of a crack or a rounded notch at room temperature, $T = 300$ K [9]. The parameters for both hydrogen diffusion and elastoplasticity were chosen relevant to low- and high-strength steel and niobium, as these systems suffer from hydrogen embrittlement, and experimental data are readily available [10–12].

2.1. Low-strength steel: rounded-notch specimen

The analysis of the rounded-notch specimen of low strength steel was modelled using the four-point-bend-specimen of Griffiths and Owen [13]. A uniform initial NILS concentration of 2.46×10^{-8} atoms per solvent atom (from Sievert's law) was used throughout as an initial condition. The outer surface of the specimen was modelled either as impermeable or was held at constant NILS concentration equal to the initial concentration. Hydrogen was assumed to expand the lattice isotropically and its partial molar volume in solution was 2.0×10^{-6} m^3 mol^{-1} [12]. The molar volume of iron was 7.116×10^{-6} m^3 mol^{-1}. The diffusion constant at 300 K was $D = 1.33 \times 10^{-8}$ m^2 s^{-1} [14]. The trap density for low strength steel was calculated as a function of plastic strain according to the experimental findings of Kumnick and Johnson [15]. The Poisson's ratio was 0.3 and Young's modulus was 207 GPa. The uniaxial stress–strain law was given by a power-law hardening relationship with a yield stress $\sigma_0 = 250$ MPa and an exponent, $N = 0.2$ [9]. The extent of deformation in the specimen was measured in terms of a nominal stress defined by $\sigma_{nom} = 6M/wa^2$, where M was the applied bending moment, a was the unnotched ligament and w was the specimen thickness. The specimen was loaded in plane strain by prescribing displacement increments. Three loading tests at constant displacement rates were performed with the displacement increasing linearly with time. Normalized nominal stress, σ_{nom}/σ_0, of 1.0, 2.0 and 3.0, with corresponding plastic strains of 0.5, 2.0 and 8.0% at the root of the notch, developed by the end of loading at time $t_l = 15$, 35, and 87 s, respectively. Subsequently the applied displacements were held constant and hydrogen diffusion continued under fixed external displacement.

In the following the hydrogen concentration profiles are plotted versus normalized distance R/r_0 along the symmetry line directly beneath the notch, where R is measured from the tip of the notch, which has a tip radius r_0. For the three loading courses, the normalized hydrogen concentration $(C_L + C_T)/C_0$ is plotted in Fig. 1 at the end of loading for both zero-flux and constant-concentration boundary conditions. Since the trap binding energy is relatively high, 60 kJ mol^{-1}, at room temperature the traps immediately saturate. Only at relatively low plastic strains, i.e. $< 0.5\%$ or equivalently for loads such that $\sigma_{nom}/\sigma_0 \leq 1.0$, is the total hydrogen population in the material dominated by the hydrostatic stress effect, that is, the peak in the hydrogen concentration occurs in from the tip. At high plastic strains, which occur when $\sigma_{nom}/\sigma_0 > 2.0$, the plastic strain effect dominates, that is, the peak of the hydrogen concentration occurs at the notch tip. It is notable that this behavior is virtually independent of the boundary conditions.

After the loading terminates and traps are no longer created, the trapped hydrogen concentration C_T/C_0 does not vary with time. However, hydrogen diffusion through NILS continues toward the hydrostatic stress peak location, and the local NILS concentration profiles continue to change at all locations until the chemical potential gradients of hydrogen are eliminated. The growth of the hydrogen concentration population and the equilibrium values are shown in Figs. 2 and 3 for two different loading cases. Again, at small plastic strains, $\sigma_{nom}/\sigma_0 \leq 1.0$, the hydrostatic stress draws the hydrogen toward the hydrostatic-stress-peak location in from the tip (Fig. 2), whereas at large plastic strains, $\sigma_{nom}/\sigma_0 > 2.0$, trapping of hydrogen at the tip dominates (Fig. 3).

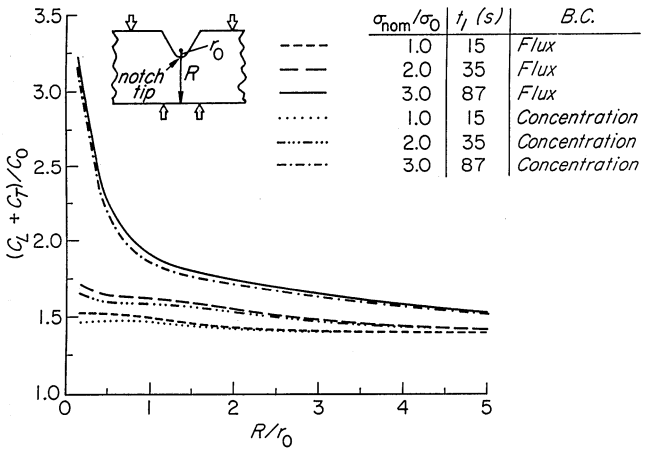

Fig. 1. Plot of total hydrogen concentration $(C_L + C_T)/C_0$ versus normalized distance R/r_0 from the notch tip in low strength steel ($\sigma_0 = 250$ MPa) at the end of loading at time t, with corresponding nominal stress σ_{nom}/σ_0 for both concentration and flux boundary conditions.

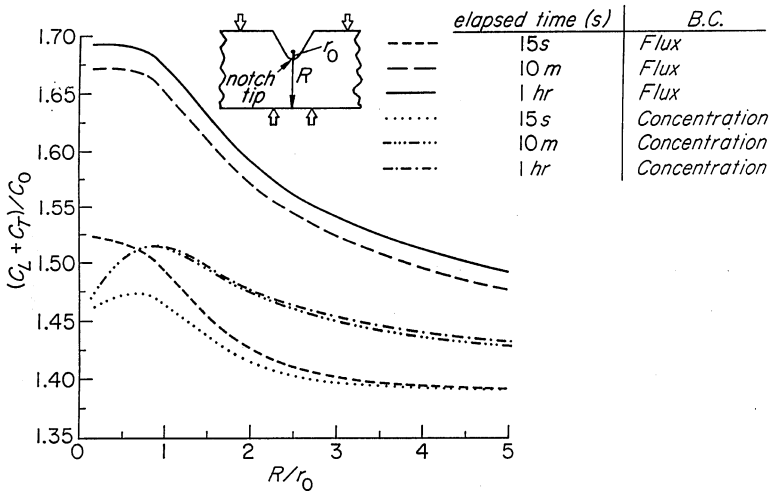

Fig. 2. Plot of total hydrogen concentration $(C_L + C_T)/C_0$ versus normalized distance R/r_0 from the notch tip in low strength steel ($\sigma_0 = 250$ MPa) at three different times during which the nominal stress σ_{nom}/σ_0 was held equal to 1.0 for both concentration and flux boundary conditions.

2.2. High-strength steel: rounded-notch specimen

Since a plastic strain of about 0.5% at the notch surface is a rather small strain in practical applications, additional calculations were carried out in the case of a high-strength steel with $\sigma_0 = 1200$ MPa and $N = 0.2$. As with low-strength iron, the problem was solved for the same domain of the rounded-notch specimen under external loads applied at a constant displacement rate in time $t_1 = 15$ s and then held fixed. At the end of loading the normalized nominal stress, σ_{nom}/σ_0, was equal to 1.0, the plastic strain at the tip of the notch was 2.3% and the maximum hydrostatic stress, $\sigma_{kk}/3\sigma_0$, was 2.0 at a distance $R/r_0 = 0.75$ from the tip. The results shown in Fig. 4 indicate that in high strength steels the hydrostatic stress dictates the shape of the hydrogen concentration profile even at plastic strains as large as 2.3%. This is due to the large magnitude of the peak hydrostatic stress ($\sigma_{kk}/3\sigma_0 = 2400$ MPa) in comparison with the corresponding small hydrostatic stress ($\sigma_{kk}/3\sigma_0 = 325$ MPa) in low-strength steels under the same normalized nominal stress of 1.0. Of course, at loads close to general yield, trapping dominates as in the case of low-strength steels.

2.3. High- and low-strength steel: blunting crack

Sofronis and McMeeking [1] modeled hydrogen transport near a blunting crack in low-strength steels, with a yield stress $\sigma_0 = 250$ MPa, a power-law hardening exponent, $N = 0.2$, at temperature 300 K and under the same concentration boundary conditions as in Section 2.1. They showed that, under small-scale-yielding conditions, hydrogen accumulates mainly in traps, and the site of accumulation of trapped hydrogen is near the crack surface, as dictated by local plasticity. Additional calculations of the present work verified that the same result is also true for the case of high-strength steels.

2.4. Niobium: blunting crack

The analysis of a blunted crack in a niobium specimen with uniform NILS hydrogen concentration, C_0, was modelled using small-scale-yielding conditions. As in the case of mild steels both constant-concentration, C_0, and zero-flux boundary conditions were investigated. The partial molar volume of hydrogen in solution in bcc niobium was $V_H = 1.88 \times 10^{-6}$ m^3 mol^{-1} and the expansion of the lattice due to hydrogen was purely dilatational [4]. The molar volume of niobium was 10.852×10^{-6} m^3 mol^{-1} and the NILS diffusion constant at 300 K was $D = 8.3 \times 10^{-10}$ m^2 s^{-1} [14]. The trap binding energy was taken 29.2 kJ mol^{-1}, as has been calculated by Baker and Birnbaum [16]. Since no experimental data for trap populations are available, the trap density was quantified through a dislocation based model for trapping. It was assumed [9] that there is one hydrogen atom trapped per atomic plane threaded by a dislocation [17], and the dislocation density was considered to vary linearly with plastic strain [18]. The Poisson's ratio was 0.39 and Young's modulus was 113 GPa. The uniaxial stress–strain law was given by a power-law hardening relationship in which $\sigma_0 = 250$ MPa and $N = 0.2$. The crack was loaded at a constant displacement rate during a loading time $t_1 = 120$ s, at the end of which the final load, phrased in terms of the applied stress intensity factor, was $K_A = 40$ MPa $\sqrt{\text{m}}$ At times greater than t, the load was kept constant at $K_A = 40$ MPa $\sqrt{\text{m}}$.

It was found that the results were independent of the boundary conditions. Fig. 5 shows that for an initial concentration of 10^{-4} H M^{-1}, i.e. hydrogen atoms per niobium atom, the total concentration is dominated by

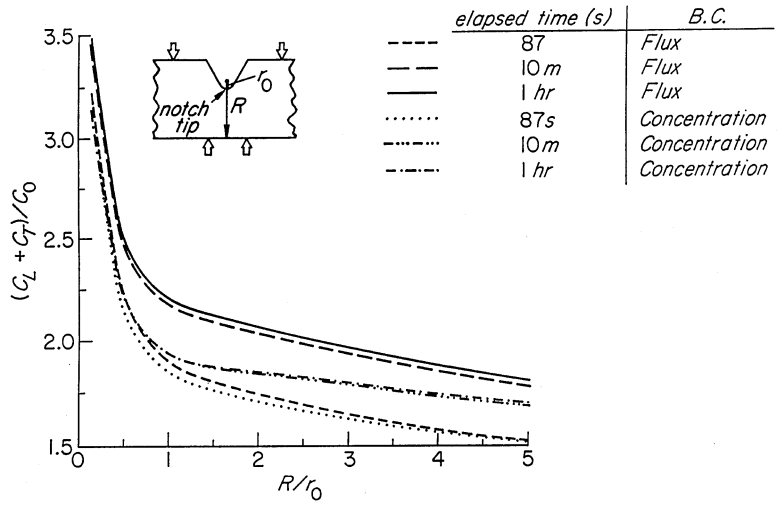

Fig. 3. Plot of total hydrogen concentration $(C_L + C_T)/C_0$ versus normalized distance R/r_0 from the notch tip in low strength steel ($\sigma_0 = 250$ MPa) at three different times during which the nominal stress σ_{nom}/σ_0 was held equal to 3.0 for both concentration and flux boundary conditions.

trapped hydrogen populations and the maximum value is attained close to the crack tip. After the loading terminates, the changes in the NILS concentration C_L are not significant, an indication that the strain rate is sufficiently slow so that near equilibrium conditions prevail during straining. When the initial concentration is much higher, i.e. 10^{-2} H M, the NILS concentrations are much greater than the trap concentrations and the hydrostatic stress dominates the hydrogen distribution at all times, as seen in Fig. 6.

3. Discussion of the results and implications for hydrogen embrittlement

It has been demonstrated that at room temperature in low-fugacity (i.e. low-solubility) systems, such as irons and low-strength steels, hydrogen accumulates mostly in regions of high plastic strain where trapping prevails, unless the plastic strain is very small. Thus, in situations of severe plastic straining, as with blunting crack tips or rounded-notch specimens with notch-root plastic strain greater than about 2.0%, the total hydrogen concentration in the region close to the crack or notch surface is always greater than the concentration at the hydrostatic-stress-peak location. However, when the plastic strain at the notch root is very small, namely about 0.5%, the calculations show that hydrogen accumulates at the hydrostatic stress-peak location inward from the tip of the notch. In general, for low-strength and low-fugacity systems the dominant hydrogen concentration and the location of the concentration peak are independent of the boundary conditions. It is notable that for round-notched, high-strength specimens of low fugacity, such as a high-strength steel, even with plastic strains as high as 2.3%, the maximum total hydrogen concentration is at the hydrostatic stress peak and not at the surface of the notch.

In high-fugacity systems, such as niobium, the site of accumulation depends strongly on the nominal concentration and the magnitude of the plastic strain. At initial concentrations H M $\leq 10^{-4}$, trapping is dominant and the peak hydrogen concentration occurs at the tip of the blunting crack. However, hydrostatic stress dictates the population distribution, even in the neighborhood of a blunting crack tip, when the initial hydrogen concentration is H M $\leq 10^{-2}$.

If a critical concentration of the hydrogen solute is required for hydrogen embrittlement to occur, the present study can help in rationalizing the location of the first cracking event [9]. The numerical results on rounded notch 4-point bend specimens will be utilized to address the location of the hydrogen-induced crack initiation site in experimental investigations of hydrogen embrittlement in steels. The hydrogen-concentration predictions are qualitative in nature, given the variability of the model parameters as they apply to a specific steel. For instance, it is not certain whether the Kumnick-and-Johnson trapping model and the associated binding energy can still be used for the kinds of steels used by other researchers in their experiments. Thus, specific model parameters and pertinent details may first need to be adjusted on a case-by-case basis to use the present model to reliably determine the hydrogen concentration at the location of the first cracking event.

Lee et al., [19,20] and Onyewenyi and Hirth [21] carried out experiments on pre-charged rounded-notch bend specimens in spheroidized AISI 1095 steel, yield stress of 380 MPa, and spheroidized AISI 1090 steel, yield stress of 345 MPa, respectively. They identified the role of hydrogen as promoting flow localization

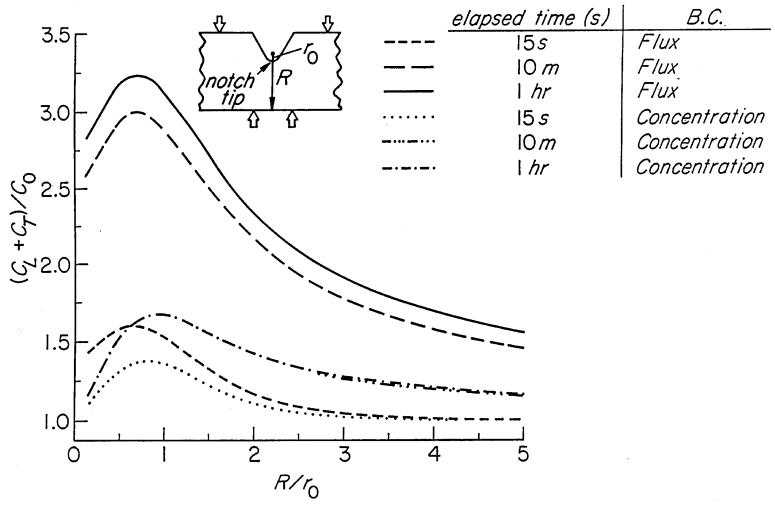

Fig. 4. Plot of total hydrogen concentration $(C_L + C_T)/C_0$ versus normalized distance R/r_0 from the notch tip in high strength steel ($\sigma_0 = 1200$ MPa) at three different times during which the nominal stress σ_{nom}/σ_0 was held equal to 1.0 for both concentration and flux boundary conditions.

(plastic instability) [5,22–24] that leads directly to crack initiation at the crack surface. The results were independent of the radius of curvature, which shows the absence of a high-triaxiality effect. In the experiments of Lee et al., [19,20], void initiation was observed at strains of 6.0%, and hydrogen enhanced the formation of deformation-induced void initiation. In the experiments of Onyewenyi and Hirth [21], it was found that at a strain of 12.0% cracking occurred at the surface of the notch and began to propagate along characteristic slip traces before any significant cracking or void formation occurred in the plastically deformed region beneath the notch root. Based on the present numerical study, these experiments represent cases of low-strength steels in which the hydrogen concentration close to the surface of the rounded notch is much larger than the concentration away from the surface.

Lee et al., [25] performed experiments on precharged U-notched specimens of tempered AISI 4340 steel, $\sigma_0 = 1280$ MPa, and found that the notch-root strain for crack initiation was at most 1.0%. They also found that MnS inclusions had little role in the fracture process. The results were interpreted to indicate that internal crack nucleation occurred at a critical combination of hydrogen concentration and local stress concentration, a result that is consistent with the decohesion theory for hydrogen embrittlement [26–35]. These results pertain to the case modelled in the present calculations in which the hydrogen concentration in high-strength steels under small strains attains its maximum at the hydrostatic-stress-peak location.

Takeda and McMahon [29] studied the hydrogen effect through tests on notched four-point-bend specimens in air and hydrogen using a 5% Ni quenched-and-

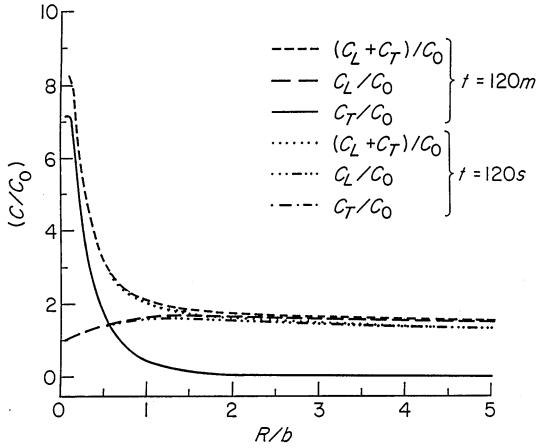

Fig. 5. Plot of hydrogen concentrations versus the normalized distance R/b in front of the crack tip in niobium at times of 120 s and 120 min. The initial NILS concentration equals 10^{-4} H/M.

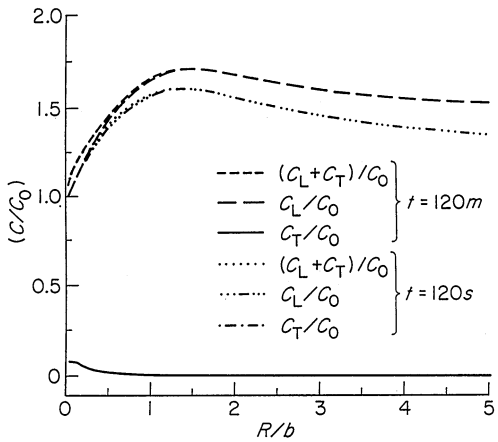

Fig. 6. Plot of hydrogen concentrations versus the normalized distance R/b in front of the crack tip in niobium at times of 120 s and 120 min. The initial NILS concentration equals 10^{-2} H/M.

tempered steel (based on HY 130). Experimenting on a specimen of yield stress $\sigma_0 = 1060$ MPa, they observed hydrogen-induced cracking along shear bands at the notch root, and they termed it plasticity-related hydrogen-induced cracking (PRHIC). It is notable that this PRHIC was observed at high strains prior to specimen failure and in the absence of sufficient impurity segregation. In this case the results of the present numerical study suggest that the preponderance of the hydrogen resides at the notch root when the plasticity is fully developed across the unnotched ligament. On the other hand, a notched specimen that had been aged for 1000 h (to allow segregation of embrittling elements, like Mn and Si, to grain boundaries), $\sigma_0 = 1015$ MPa, microcracked intergranularly at a load less than half of the general yield load in the region between the notch tip and the hydrostatic-stress-peak location. According to the present calculations for high-strength steels, the location of maximum hydrogen accumulation is inward from the notch root at the hydrostatic-stress location when the plasticity is limited.

In summary, the finite-element calculations of the maximum hydrogen accumulation site ahead of a rounded notch subjected to stress are in correspondence with experimental findings on the location of the crack-initiation site. When fracture is accompanied by large strains at the notch root, most of the hydrogen is trapped close to the notch root, and cracking has been observed to initiate there. In contrast, when limited plastic straining precedes the fracture event, most of the hydrogen resides at the NILS sites at the hydrostatic-stress-peak location inward from the tip. At these occasions hydrogen has been reported to induce microcracking in the highly stressed material volume inside from the notch root.

4. Conclusion

A methodology has been developed to study the mechanical interaction of hydrogen with plastic strain and stress as a function of temperature, loading conditions and material parameters in the neighborhood of stress raisers. This type of analysis can be used to understand various aspects of the complex phenomenology of hydrogen embrittlement.

In experimental studies with 4-point bend specimens, hydrogen-induced cracking at the surface of the notch occurred under large strains, and microcracking inward from the notch was the case at very small strains. These results, in conjunction with the present numerical calculations of the hydrogen concentration, suggest that most of the hydrogen was residing at the microcrack-initiation site prior to the onset of fracture. Therefore, a critical hydrogen concentration may be a necessary condition for hydrogen embrittlement; this merits further investigation [36]

Acknowledgements

This work was supported by the Department of Energy under grant DEFGO2-91ER45439.

References

[1] P. Sofronis, R.M. McMeeking, J. Mech. Phys. Solids 37 (1989) 317.
[2] H.H. Johnson, R.W. Lin, in: I.M. Bernstein, A.W. Thompson (Eds.), Hydrogen Effects in Metals, Metallurgical Society of AIME, New York, 1981, pp. 3–23.
[3] R. Hill, The Mathematical Theory of Plasticity, Oxford University Press, NY, 1985.
[4] H. Peisl, in: G. Alefeld, J. Volkl (Eds.), Hydrogen in Metals I, Topics in Applied Physics, vol. 28, Springer-Verlag, New York, 1978, 53–74.
[5] P. Sofronis, H.K. Birnbaum, J. Mech. Phys. Solids 43 (1995) 49.
[6] J. Lufrano, P. Sofronis, Int. J. Solids Structures 33 (1996) 1709.
[7] J. Lufrano, Hydrogen transport in hydride and non-hydride forming metals and the mechanistic implications for fracture behavior, Ph.D. dissertation, University of Illinois at Urbana-Champaign, Urbana, IL, 1996.
[8] R.M. Govindarajan, N. Aravas, Int. J. Mech. Sci. 36 (1994) 343.
[9] J. Lufrano, P. Sofronis, Acta Mater. 46 (1998) 1519–1526.
[10] F.M. Mazzolai, H.K. Birnbaum, J. Phys. F: Met. Phys 15 (1985) 507.
[11] F.M. Mazzolai, H.K. Birnbaum, J. Phys. F: Met. Phys 15 (1985) 525.
[12] J.P. Hirth, Metall. Trans. A 11 (1980) 861.
[13] J.R. Griffiths, D.R.J. Owen, J. Mech. Phys. Solids 19 (1971) 419.
[14] J. Volkl, G. Alefeld, in: G. Alefeld, J. Volkl (Eds.), Hydrogen in Metals I, Topics in Applied Physics, vol. 28, Springer-Verlag, New York, 1978, pp. 321–348.
[15] A.J. Kumnick, H.H. Johnson, Acta Metall. 28 (1980) 33.
[16] C. Baker, H.K. Birnbaum, Scr. Met. 6 (1972) 851.
[17] J.K. Tien, A.W. Thompson, I.M. Bernstein, R.J. Richards, Metall. Trans. A 7 (1976) 821.
[18] J.J. Gilman, Micromechanics of Flow in Solids, McGraw-Hill, New York, 1969, pp. 185–199,
[19] T.D. Lee, T. Goldenberg, J.P. Hirth, Metall. Trans. A 10 (1979) 199.
[20] T.D. Lee, T. Goldenberg, J.P. Hirth, Fracture 1977, vol. 2, University of Waterloo Press, Waterloo, 1977, pp. 243–248.
[21] O.A. Onyewenyi, J.P. Hirth, Metall. Trans. A 14 (1983) 259.
[22] H.K. Birnbaum, P. Sofronis, Mat. Sci. Eng A 176 (1994) 191.
[23] E. Sirois, H.K. Birnbaum, Acta Metall. 40 (1992) 1377.
[24] E. Sirois, P. Sofronis, H.K. Birnbaum, in: S.M. Bruemmer, E.I. Meletis, R.H. Jones, W.W. Gerberich, F.P. Ford,, R.W. Staehle (Eds.), Parkins Symposium on Fundamental Aspects of Stress Corrosion Cracking, The Minerals, Metals and Materials Society, 1992, pp. 173–190.
[25] T.D. Lee, T. Goldenberg, J.P. Hirth, Metall. Trans. A 10 (1979) 439.
[26] A.R. Troiano, Trans. ASM 52 (1960) 54.
[27] H.H. Johnson, J.G. Morlet, A.R. Troiano, Trans. Met. Soc. AIME 212 (1958) 528.
[28] E.A. Steigerwald, F.W. Schaller, A.R. Troiano, Trans. Met. Soc. AIME 218 (1960) 832.
[29] Y. Takeda, C.J. McMahon Jr., Metall. Trans. A 12 (1981) 1255.
[30] X. Chen, T. Foecke, M. Lii, Y. Katz, W.W. Gerberich, Eng. Fracture Mech. 35 (1990) 997.
[31] M.J. Morgan, Grain boundary segregation and embrittlement by antimony and hydrogen in a model alloy steel, PhD dissertation, University of Pennsylvania, Philadelphia, Pennsylvania, 1987.

[32] R.A. Oriani, P.H. Josephic, Acta Metall. 22 (1974) 1065.
[33] R.A. Oriani, P.H. Josephic, Acta Metall. 25 (1977) 979.
[34] W.W. Gerberich, Y.T. Chen, Metall. Trans. A 6 (1975) 271.
[35] J.F. Lessar, W.W. Gerberich, Metall. Trans. A 7 (1976) 953.
[36] D.F. Teter, The effects of hydrogen on the deformation and fracture behavior of the metastable beta-titanium alloy, timetal 21 S, PhD dissertation, University of Illinois at Urbana-Champaign, Urbana, Illinois, 1996.